Orbital and spin-polarization transfer in ionizing electron-atom collisions

J. Lower and E. Weigold
Atomic and Molecular Physics Laboratories, Research School of Physical Sciences and Engineering, Australian National University, Canberra ACT 0200, Australia

J. Berakdar
Max-Planck Institute for Microstructure Physics, Weinberg 2, 06120 Halle, Germany

S. Mazevet
T-division, Los Alamos National Laboratory, Los Alamos, New Mexico 87545
(Received 19 March 2001; published 10 September 2001)

We have performed an experiment in which a polarized electron beam ionizes an orbitally oriented and/or spin-polarized valence electron of sodium. The cross section for this reaction is measured for well-resolved vector momenta of the two electrons in the final channel. In order to study the transfer of the initial spin and orbital orientation from the electron-atom system to the final-state correlated electron pair, we develop a tensorial recoupling scheme in which the measured quantities are expressed in terms of independent, irreducible spherical tensor components. By this procedure the cross section is separated into terms characterized by their specific rotational transformation properties, decoupling of geometrical effects due to initial-state preparation from effects associated with details of the scattering dynamics is achieved, and exchange and orbital angular momentum transfer effects are disentangled. For a comparison with experiment we performed numerical ionization-cross section calculations within the distorted wave Born approximation and the dynamically screened three Coulomb waves theory. For some tensorial parameters significant discrepancies between theory and experiment are observed that underline the importance of the state-specific measurements as stringent tests of scattering theories.

DOI: 10.1103/PhysRevA.64.042701 PACS number(s): 34.80.Dp, 34.80.Nz, 34.80.Qb

I. INTRODUCTION

The behavior of electrons determines decisively a wide range of properties of materials such as their resistivity and their optical response. While in most cases the ground state is efficiently deduced via minimizing the energy, the treatment of excited states still poses a challenge both conceptually and computationally [1]. In principle, the excitation spectrum is determined by the energy, momentum, and spin transfer during collisions between the constituents of the system. Thus the question arises as to what extent we are able to describe theoretically electronic collisions and which experimental ways and tools are necessary to judge the quality of theory. Obviously, the simplest case to start from is a system of two colliding electrons with well-defined moderate energies. Here the determining factors are the electrostatic scattering potential known analytically and the exchange interaction that originates from the Pauli exclusion principle. Fortunately, the two-body Coulomb scattering problem can be solved analytically [2,3]. However, for three-particle systems, e.g., an electron colliding with a one-electron atom (hereafter referred to as the *e*-atom system), the situation changes in two ways. The total potential that governs the system's dynamics has a richer structure, such as the existence of saddle points and nonmonotonic potential gradients and in the electron-atom collision case, in contrast to two-body scattering, the electron bound to the atom may have a well-defined orbital momentum with known sense of circulation (magnetic quantum numbers). Recently it has been shown that these additional degrees of freedom influence the dynamics of the scattering process [4–7].

Thus the goals of a many-body scattering theory are the treatment of the charge scattering dynamics as dictated by the total potential, the modeling of the spin scattering processes constrained by the Pauli principle and/or influenced by additional spin-dependent forces, and the isolation of the role of the orbital degrees of freedom.

Basically these questions and the fundamental aspects of the physical processes remain unaltered when dealing with more complex correlated systems, such as ferromagnets (exchange interaction) [8] or heavy-fermion systems [the (de-)coupling between charge, spin, and orbital degrees of freedom] [1]. Therefore, it is desirable to develop a general theoretical scheme based on symmetry arguments and hence applicable to systems beyond the atomic case.

For a detailed probe of the scattering dynamics and the theoretical approaches new experimental techniques are necessary. In this work an experimental arrangement is presented that probes the spin, the orbital, and the charge dependence of electron-atom ionizing collisions. This is achieved by performing ionization coincidence measurements in which both the spin and the orbital projection quantum states of the electron-atom system are determined prior to the collision, as well as the energies and momenta of the projectile and the two final-state continuum electrons.

Sodium was chosen as the target in the present study for a number of reasons. First, it possesses a simple hydrogenlike structure that enables a simplified treatment of the many-body scattering to be performed. Second, it is a light atom, the consequence of which is that spin-orbit interaction between the continuum electrons in the initial and final states

and the target (ion) can be neglected, enabling the results of experiment to be interpreted solely in terms of orbital angular momentum and electron exchange effects. In contrast, if a heavy target atom were used, this continuum spin-orbit interaction would lead to an additional dependence, for both ground- and excited-state transitions, of the measured cross section on the absolute orientations of both bound and continuum electron-spin projections, a complication avoided by the present choice of target. Finally, to achieve a well-defined sense of circulation of the valence electron we utilize laser pumping for the $3s$-$3p$ sodium transition. Through this procedure a target ensemble comprising both spin-polarized ground-state and spin-polarized and oriented excited-state atoms is achieved. The details of this pumping process are well understood and the transition occurs in a frequency range that is easily accessible to high-power tunable lasers.

The ionization measurements presented here on spin-polarized ground-state sodium atoms using a spin-polarized electron beam enables the process of exchange to be sensitively probed. This is because for a light atom such as sodium it can be safely assumed that spin-flip processes are negligible and the only spin-dependent effects observed will be due to exchange. Furthermore, complications arising from finite-target orientation, which for the excited $3p$ state influence the cross sections for ionization, are avoided. Thus the ionization cross sections depend only on the relative spin orientations of the projectile and target electrons before the collision.

The exchange interaction can be most easily analyzed by extracting from the measurement the individual cross sections leading to a vanishing total spin state $S=0$ (singlet scattering) and to a $S=1$ state (triplet scattering). These measurements are similar to the pioneering work of Baum and co-workers [9–11] for the scattering of spin-polarized electrons from spin-polarized ground-state lithium atoms.

In contrast, the ionization results for the oriented $3p$ excited states enable the role of orbital orientation to be probed. Orientation is defined as the expectation value of the orbital angular momentum operator along an arbitrary quantization axis [12]. The dependence of the electron-impact ionization cross section [$(e,2e)$ cross section] on target orientation, for the case of an unpolarized beam of electrons, has been described previously [4,5]. In the present case, for spin-polarized primary electrons, it is shown that the singlet and triplet partial cross sections deduced from experiment also exhibit a dependence on target orientation. It should be noted that the experiments on $3s$ and $3p$ ionization are performed simultaneously under identical experimental conditions as the target ensemble comprises both ground- and excited-state atoms.

To disentangle the spin-dependent from the orbital orientation effect we employed a tensorial recoupling scheme in which the cross sections are expressed in terms of independent, irreducible spherical tensor components. Each of the components has a well-specified behavior (determined by the rank of the respective tensor) under rotations generated by the spin or orbital angular momentum. This permits an identification of the exchange-induced and orbital orientation effects on symmetry grounds without resorting to numerical calculations. In addition, this method allows a decoupling of the geometrical effects due to initial-state preparation from those dependent upon the scattering dynamics.

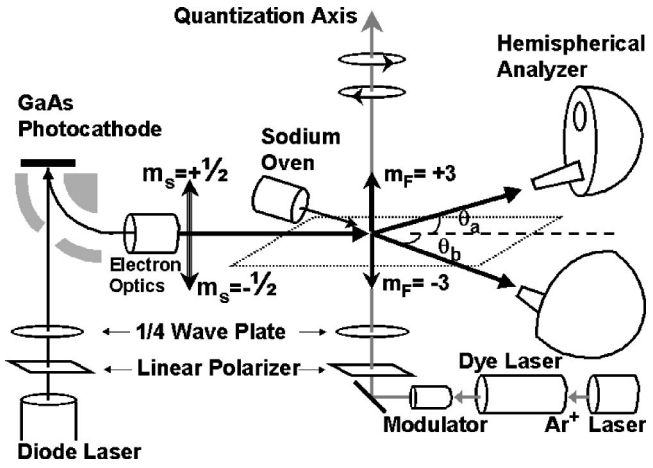

FIG. 1. Schematic representation of the $(e,2e)$ experiment on laser pumped sodium atoms. Pairs of electrons liberated from ionization of ground-state $3s$ and excited-state $3p$ orbitals are measured in two hemispherical electrostatic energy analyzers. See text for details.

For comparison with experiment, numerical values for the tensorial components are needed. For this numerical study we utilize the distorted wave Born approximation (DWBA) [3,13] and the dynamically screened three Coulomb waves (DS3C) theory [14]. For some tensorial parameters significant discrepancy between theory and experiment is observed. This might be due to an insufficient modeling of the sodium atom and/or a shortcoming in describing the complete scattering dynamics.

The paper is organized as follows. Section II describes the methods used to perform the present measurements and provides a description of the apparatus. The reaction kinematics and the laser pumping techniques used to prepare the initial quantum state of the primary electron and target are also explained. In Sec. III the theoretical methodology used in this work is presented. Tensorial parameters are introduced to highlight the physical aspects of the collision process. Expressions relating these parameters to experimentally determined count rates are presented. Following this discussion, the results of the DWBA [13] and DS3C method [14] and other calculational schemes are presented and discussed in light of the experimental data. Section IV concludes by summarizing the main results of the study and points to ways in which future improvements in theory and experiment will be achieved.

II. EXPERIMENTAL METHODOLOGY

Figure 1 shows schematically the kinematical arrangement employed for the present measurements and the main components of the apparatus. As a detailed description of the apparatus has appeared in previous publications [5,15], only a brief description will be given here.

Electron impact ionization events occur within the collision volume, defined as the region of space formed by the

intersection of the sodium, primary electron, and the dye laser beams. The sodium target beam is produced by effusion through a 1-mm-diameter exit nozzle of an ohmically heated recirculating sodium oven and collimated by a liquid-nitrogen-cooled aperture. The oven is mounted on a turntable rotatable about the dye laser beam axis. After passing through the interaction region the sodium beam is condensed on a liquid-nitrogen-cooled beam dump (not shown in figure) mounted from the oven. Rotational freedom of the oven and dump allows the scattered electron analyzers to access angular regions that would otherwise remain obscure.

The primary polarized-electron beam used to induce the ionization process is generated by photoemission from a cesium- and oxygen-coated GaAs crystal under illumination by 810 nm circularly polarized laser radiation. This radiation field is derived from passing linearly polarized light from a 3-mW diode laser through a rotatable quarter-wave-plate interposed between the diode laser and GaAs photocathode. Details of the crystal cleaning and surface preparation procedure used in the present work can be found in Ref. [5]. The degree of polarization P_e achieved for the present measurements was 0.24 ± 0.03 and remained stable over the duration of the measurements. Inversion of the electron beam polarization from into, to out of the scattering plane is achieved by reversing the helicity of the diode laser radiation field through rotation of a quarter-wave plate.

A frequency-modulated 589 nm circularly polarized laser beam is used to excite, spin polarize, and in the case of the excited-state atoms, additionally orient the sodium target ensemble. This is achieved through pumping the $3s$-$3p$ transition by circularly polarized light. Through the actions of an electro-optical modulator, the single-mode dye laser beam is frequency modulated, causing side bands to appear in the laser frequency spectrum. This enables excitation to be performed by means of two laser frequencies and results in an improved excitation fraction of around 40% [16]. After a few excitation/decay cycles the target atoms gather exclusively in the two-state system

$$3s^1{}^2S_{1/2}(F=2, m_F=+2(-2)) \leftrightarrow 3p^1{}^2P_{3/2}(F=3, m_F=+3(-3)) \quad (1)$$

for pumping by left-hand σ^+ (right-hand σ^-) circularly polarized radiation.

The ground states $(F=2, m_F=+2(-2))$ consist of maximum projections of electron spin $m_S=+1/2(-1/2)$ and correspond to a target polarization directed out of (into) the scattering plane. The two excited states $(F=3, m_F=+3(-3))$ consist of maximum projections of both electron spins $m_S=+1/2(-1/2)$ and orbital angular momentum $m_L=+1(-1)$ (and nuclear spin $I=3/2$). For this case the associated target polarization and orientation vectors are parallel to one another and directed out of (into) the scattering plane.

Scattered electrons, which are emitted in the scattering plane defined by the momentum vectors of the sodium and primary electron beams, are measured in two electrostatic hemispherical analyzers located on opposite sides of the incident beam. Each analyzer is mounted on its own turntable that is, as for the oven turntable, independently rotatable about the dye laser beam axis that defines the quantization axis in the present measurements. Microchannel plate electron multipliers and resistive anode-position-sensitive detectors are incorporated into the exit plane of each analyzer and enable simultaneous measurement of electron energies over a 6 eV band and with a resolution of around 300 meV. $(e,2e)$ events, corresponding to the emission of two electrons from a common ionization event, are identified by the correlated arrival times of an electron detected in each of the two separate microchannel plate detectors. Events corresponding to the random emission of two electrons from separate scattering events, but detected within the instrumental $(e,2e)$ timing resolution, are subtracted using standard statistical techniques [17].

The experiments consisted of measuring the $(e,2e)$ count rates as a function of the emission angle θ_b of one of the two final-state electrons, for a fixed emission angle θ_a of the other, for each of the four combinations of atomic and electron-beam polarization directions. For ground-state ionization, measurements were performed for the following four reactions:

$$e(\uparrow)+\mathrm{Na}(m_F=+2), \quad e(\uparrow)+\mathrm{Na}(m_F=-2),$$

$$e(\downarrow)+\mathrm{Na}(m_F=+2), \quad e(\downarrow)+\mathrm{Na}(m_F=-2), \quad (2)$$

and for excited-state ionization for the reactions,

$$e(\uparrow)+\mathrm{Na}(m_F=+3), \quad e(\uparrow)+\mathrm{Na}(m_F=-3),$$

$$e(\downarrow)+\mathrm{Na}(m_F=+3), \quad e(\downarrow)+\mathrm{Na}(m_F=-3). \quad (3)$$

The ground- and excited-state measurements were performed simultaneously since the atomic target consisted of a known fraction of excited- and ground-state atoms. The above four measurements were made for equal times at each angle θ_b before changing to a new angle θ_b. The accessible range of θ_b, which was contingent upon the relative positions of both analyzers and the sodium oven, varied from experiment to experiment but always lay between 40° and 90°. The full range of angles θ_b was swept through many times in each experiment to average over instrumental drifts with measurements being performed at 5° intervals.

In order to discriminate between ionization events resulting from the removal of $3s$ and the $3p$ electrons, respectively, the binding energy ϵ_I of the ejected electron is deduced from the energies of the two final-state continuum electrons, E_a and E_b respectively, and the energy E_0 of the incoming electron through the relation

$$\epsilon_I = E_0 - (E_a + E_b). \quad (4)$$

For each measured coincidence event the energies E_a and E_b of both detected outgoing electrons is summed and stored on a multichannel analyzer. In our notation $E_a \geqslant E_b$. From this a binding-energy spectrum is formed with an energy

resolution given by the convolution of the energy spread of the incoming beam and the apparatus functions of both of the electron analyzers. In the present case, an $(e,2e)$ binding energy resolution of around 0.9 eV was achieved, more than sufficient to discriminate between events corresponding to ionization of the ground-state $\epsilon_I(3s)=5.14$ eV and excited-state atoms $\epsilon_I(3p)=3.0$ eV.

An energy average was performed at each value of binding energy over all combinations of values for E_a and E_b within the 6 eV acceptance band of each analyzer, which satisfy Eq. (4). Both analyzers possess a flat energy response to a very good approximation. In this way the results could be displayed in a more compact form and the statistics at each data point improved. Accordingly, the symbols $\overline{E_a}$ and $\overline{E_b}$ are used to denote the 6-eV energy-averaged values (also the mean energies) for the two final-state continuum electrons. All calculations presented in this paper have likewise been energy averaged over 6 eV to enable a valid comparison with experiment to be made.

It should also be noted that in each of the three experimental data sets presented here, performed at a fixed value of incident energy, the difference in binding energy between $3s$ and $3p$ electrons reflects itself in 1-eV lower values for the mean scattered electron energies $\overline{E_a}$ and $\overline{E_b}$ for the ground, as compared to the excited-state data.

In the present measurements, data were collected under three separate kinematical conditions, each characterized by a particular choice of initial- and final-state electron momenta and designed to highlight different aspects of the ionization process.

The first experiment was performed at an incident energy of 151 eV under highly asymmetric scattering kinematics. Under such conditions, one anticipates exchange effects to play a minor role. Here the fast scattered electron was of average energy $\overline{E_a}=127$ eV for $3p$ ionization and measured at a fixed scattering angle $\theta_a=20°$. This corresponds closely to the binary collision region (or Bethe ridge kinematics), i.e., scattering from a stationary free electron.

The second measurement was performed under conditions of symmetric energy sharing between the two final-state electrons at an incident beam energy of 83 eV. Under such conditions exchange effects are expected to be strong. This reaction kinematics also encompasses the condition where both final-state electrons possess identical energies and scattering angles (on opposite sides of the primary beam), which allows basic symmetry properties relating to exchange and orbital angular momentum transfer to be tested.

The final measurement was performed at an even lower value of incident energy (64 eV), with the average fast scattered electron energy $\overline{E_a}$ of 40.5 eV for $3p$ ionization. Under these conditions of low final-state energies, correlation effects involving the mutual interactions between the three charged particles liberated through the ionization process are enhanced, providing theory with a particularly difficult challenge to accurately describe this aspect of the ionization process.

III. THEORETICAL FORMULATION

A. Tensorial recoupling

For a general formulation we consider the ionization of a mixed state of a quantum system for which the total orbital momentum J is a good quantum number. The system can be characterized by a density matrix ρ. The matrix elements of ρ in an angular momentum basis are given by

$$\langle JM|\rho|JM'\rangle=\sum_{K=0}^{2J}\sum_{m_K=-K}^{K}(-1)^{J-M}\langle JM'J-M|Km_K\rangle P_{Km_K}. \tag{5}$$

Here we assume that the states with $J'\neq J$ do not contribute to the statistical mixture. The irreducible components P_{Km_K} of the density matrix are called the *polarization momenta* [18] and are related to the standard polarization state multipoles ρ_{Km_K} (that we employed in [19,4,5]) by $P_{Km_K}=\rho^*_{Km_K}$.

The components P_{Km_K} satisfy the following relations:

$$P^*_{Km_K}=(-1)^{m_K}P_{K-m_K} \tag{6}$$

$$P^*_{Km_K}=c_K\langle\{\mathbf{J}\}_{Km_K}\rangle, \tag{7}$$

where $\langle\{\mathbf{J}\}_{Km_K}\rangle$ denotes an averaged value of the tensor product of angular momentum operators $\mathbf{J}$. The constant c_K is given by the formula

$$c_j=2^j\sqrt{\frac{(2j+1)!!(2J-j)!}{j!(2J+j+1)!}}.$$

In a recent paper [20] useful representations are given for P_{Km_K} in terms of the averaged values of the components of $\mathbf{J}$.

For the description of the ensemble of the incoming polarized electron beam we employed the density matrix elements $\overline{\rho^s}_{m_sm'_s}$. These can be expanded in the same manner as done in Eq. (5):

$$\overline{\rho^s}_{m_sm'_s}=\sum_{k=0}^{2s}c_k\sum_{m_s=-k}^{k}(-1)^{s-m_s}\langle sm'_s s-m_s|km_k\rangle\langle\{\mathbf{s}\}_{km_k}\rangle=\sum_{k=0}^{2s}\sum_{m_s=-k}^{k}(-1)^{s-m_s}\langle sm'_s s-m_s|km_k\rangle p_{km_k}. \tag{8}$$

Following the ionization of the atomic mixture by the incoming electron beam two electrons are transferred into the continuum and emerge with energies E_a and E_b and emission solid angles Ω_a and Ω_b. The cross section $\sigma(\Omega_a,\Omega_b,E_b)$ for this process is given by

$$\sigma(\Omega_a,\Omega_b,E_b)=C\sum_{SM_S}\sum_{\substack{MM'\\ mm'}}\langle\chi_{SM_S}\Psi_{\mathbf{k}_a\mathbf{k}_b}|V|\varphi_{\mathbf{k}_0m_s}\Phi_{JM}\rangle \times\rho^{J}_{MM'}\overline{\rho^{s}_{m_sm_s'}}\langle\Phi_{JM'}\varphi_{\mathbf{k}_0m_s'}|V|\chi_{SM_S}\Psi_{\mathbf{k}_a\mathbf{k}_b}\rangle, \tag{9}$$

where $|\varphi_{\mathbf{k}_0m_s}\Phi_{JM}\rangle$ is an undistorted initial state consisting of a bound state $|\Phi_{JM}\rangle$ and a spinor plane wave $|\varphi_{\mathbf{k}_0m_s}\rangle$ with an incident momentum $\mathbf{k}_0$. The state vector $\langle\chi_{SM_S}\Psi_{\mathbf{k}_a\mathbf{k}_b}|$ represents an antisymmetrized two-electron state with a total spin S, total spin projection M_S, and possessing appropriate boundary conditions that describes two escaping electrons with asymptotic momenta $\mathbf{k}_a$ and $\mathbf{k}_b$.

In Eq. (9) the constant $C=(2\pi)^4k_ak_b/k_0$ is a kinematical factor (due to normalization to the incident flux current density). The operator that induces the transition is the projectile-target interaction V and is assumed in the rest of this work to be spin independent. For simplicity we choose situations for which the structure of the final residual-ion state is irrelevant to the present $(e,2e)$ reaction.

With Eq. (6) the expression (9) can be written as

$$\begin{aligned}\sigma(\Omega_a,\Omega_b,E_b)=C\sum_{K=0}^{2J}\sum_{m_K=-K}^{K}\sum_{k=0}^{2s}\sum_{m_k=-k}^{k}c_kc_K\langle\{\mathbf{J}\}_{Km_K}\rangle\\ \times\langle\{\mathbf{s}\}_{km_k}\rangle\sum_{SM_S}\sum_{\substack{MM'\\ m_sm_s'}}(-1)^{J-M+s-m_s}\\ \times\langle JM'J-M|Km_K\rangle\langle sm_s's-m_s|km_k\rangle\\ \times\langle\chi_{SM_S}\Psi_{\mathbf{k}_a\mathbf{k}_b}|V|\varphi_{\mathbf{k}_0,m_s}\Phi_{JM}\rangle\\ \times\langle\Phi_{JM'}\varphi_{\mathbf{k}_0,m_s'}|V|\chi_{SM_S}\Psi_{\mathbf{p}_a,\mathbf{p}_b}\rangle.\end{aligned} \tag{10}$$

Thus we arrive at the compact expression

$$\begin{aligned}\sigma(\Omega_a,\Omega_b,E_b)=\sum_{K=0}^{2J}\sum_{m_K=-K}^{K}\sum_{k=0}^{2s}\sum_{m_k=-k}^{k}c_kc_K\langle\{\mathbf{J}\}_{Km_K}\rangle\\ \times\langle\{\mathbf{s}\}_{km_k}\rangle\sum_{SM_S}\Lambda^{Kk}_{m_Km_k}(SM_S),\end{aligned} \tag{11}$$

where $\Lambda^{Kk}_{m_Km_k}(SM_S)$ is a tensor of rank K with spherical components m_K. In addition, $\Lambda^{Kk}_{m_Km_k}(SM_S)$ can be considered as a tensor of rank k with components m_k. To prove this statement we may proceed by defining the quantities $\mathcal{M}^{J}_{M'}=\langle\Phi_{JM'}\varphi_{\mathbf{k}_0,m_s'}|V|\chi_{SM_S}\Psi_{\mathbf{k}_a,\mathbf{k}_b}\rangle$. Since the dependence of $\mathcal{M}^{J}_{M'}$ on M' is given by the M' dependence of angular momentum eigenstates $(|\Phi_{JM'}\rangle)$ we can consider $\mathcal{M}^{J}_{M'}$ as a spherical tensor of rank J with spherical components being indexed by M'. In addition, we can write the complex conjugate in the form $(\mathcal{M}^{J}_{M})^*=(-1)^{\alpha-M}\mathcal{W}^{J}_{-M}$. This relation defines the tensor $\mathcal{W}^{J}_{-M}$ of rank J and components M and resembles formally the definition of the adjoint of a tensor operator where the phase α is arbitrary but satisfies the constraint that $\alpha-M$ is an integer. With these definitions we find for $\Lambda^{Kk}_{m_Km_k}$ under an appropriate choice for α $(\alpha=-J)$

$$\begin{aligned}\Lambda^{Kk}_{m_Km_k}=C\sum_{m_sm_s'}(-1)^{s-m_s}\langle sm_s's-m_s|km_k\rangle\\ \times\sum_{M'M}\langle JM'J-M|Km_K\rangle\mathcal{M}^{J}_{M'},\mathcal{W}^{J}_{-M}.\end{aligned} \tag{12}$$

The sum over M and M' is equivalent to the definition of the standard tensor product of two tensors of rank J to yield a tensor (Λ^K) of rank K. Obviously, this procedure and conclusions can be repeated for the sum over m_s and m_s'.

The formal conclusion that $\Lambda^{Kk}_{m_Km_k}$ is a spherical tensor has immediate consequences as far as the rotational transformation properties are concerned. Tensors with rank $K=0$ and/or $k=0$ are scalar with respect to rotations generated by $\mathbf{J}$ and/or $\mathbf{s}$. The tensors with rank $K=$ odd ($k=$ odd) are orientation parameters whereas for $K=$ even ($k=$ even) the tensors can be regarded as alignment tensors [12].

The relation (11) is valid for an arbitrary mutual angle between the natural quantization axes of the incoming electron beam and the polarized atomic target. If the polarized electron beam and the polarized target have a common quantization axis (as is the case in the present experiment) the density matrices become diagonal and Eqs. (11) reduce to

$$\begin{aligned}\sigma(\Omega_a,\Omega_b,E_b)=\Lambda^{0,0}_{0,0}\Bigg[P_{00}p_{00}+P_{00}p_{10}\frac{\Lambda^{0,1}_{0,0}}{\Lambda^{0,0}_{0,0}}\\ +\sum_{K=1}^{2J}\Bigg(P_{(K=\text{odd})0}p_{00}\frac{\Lambda^{(K=\text{odd}),0}_{0,0}}{\Lambda^{0,0}_{0,0}}\\ +P_{(K=\text{odd})0}p_{10}\frac{\Lambda^{K=\text{odd},1}_{0,0}}{\Lambda^{0,0}_{0,0}}\Bigg)\\ +\sum_{K=2}^{2J-1}\Bigg(P_{(K=\text{even})0}p_{00}\frac{\Lambda^{(K=\text{even}),0}_{0,0}}{\Lambda^{0,0}_{0,0}}\\ +P_{(K=\text{even})0}p_{10}\frac{\Lambda^{(K=\text{even}),1}_{0,0}}{\Lambda^{0,0}_{0,0}}\Bigg)\Bigg].\end{aligned} \tag{13}$$

The first term of the sum in Eq. (13) yields the spin-averaged cross section from randomly oriented targets, whereas the second term is the spin asymmetry for the ionization of isotropic targets by polarized electrons. The third term describes the orientational asymmetries (dichroism) averaged over the spin polarization of the incident beam whereas the fourth term represents a spin and orbital asymmetry. The fifth (sixth) term is to be associated with spin-averaged (spin-resolved) alignment parameters.

B. Applications to the present experiment

From Eq. (12) it is clear that for an evaluation of $\Lambda^{K,k}_{m_K m_k}$ one has to calculate the spin- and initial-state-resolved cross sections σ_{JM,m_s}. To describe the present experiment we can discard the spin-orbit interaction (in all channels). The spin and orbital degrees of freedom are then decoupled and the cross sections σ_{JM,m_s} are easily related to the ionization cross sections σ_{LM_L,m_s}, where L is the orbital angular momentum and M_L is its projection along the atomic quantization axis. For the experimental arrangement shown in Fig. 1 the ionization cross section for the orbital $m_L=0$ is zero [19]. Therefore (and due to the neglect of any spin-flip reactions) only four (out of eight) parameters in Eqs. (13) are independent. These are Λ^{00}_{00}, Λ^{10}_{00}, Λ^{01}_{00}, and Λ^{11}_{00}. As done in Eq. (13) we can reexpress these quantities in terms of asymmetry parameters. This is particularly useful as the individual cross sections σ_{JM,m_s} are measured on a relative scale but the absolute value of the ratio of cross sections $\sigma_{JM,m_s}/\sigma_{JM',m'_s}$ $(M\neq M', m_s\neq m'_s)$ are determined.

In the following description we use the notation $N^{\uparrow\Uparrow}$ $(N^{\downarrow\Uparrow})$ to describe the *measured* count rates for ionization when the target volume is pumped by left-hand $\Uparrow$ circularly polarized radiation and ionized by an electron beam whose polarization vector is out of $\uparrow$ (or into $\downarrow$) the scattering plane. In the same manner $N^{\downarrow\Downarrow}$ $(N^{\uparrow\Downarrow})$ represents count rates when the target atoms are pumped by right-hand $\Downarrow$ circularly polarized laser light and ionized by an electron beam whose polarization vector is into $\downarrow$ (or out of $\uparrow$) the scattering plane.

C. Ionization from the spin-polarized ground state

For the ground-state ionization $(J=1/2, s=1/2)$ we deduce from Eq. (13) that four independent parameters $\Lambda^{Kk}_{00}, K,k=0,1$ can be measured. However, as we have neglected any spin-flip processes the parameters Λ^{01}_{00} and Λ^{10}_{00} vanish and the remaining two parameters Λ^{00}_{00} and Λ^{11}_{00} will be given below in terms of the measured state-resolved triplet and singlet cross sections [see Eqs. (28)].

The ionization cross section depends only on the *relative* spin orientations of the projectile and target beams. For this reason count rates corresponding separately to parallel ($N^{\uparrow\Uparrow}$ and $N^{\downarrow\Downarrow}$) and antiparallel ($N^{\downarrow\Uparrow}$ and $N^{\uparrow\Downarrow}$) spins can be summed. The two partial cross sections σ_s and σ_t, corresponding respectively to ionization leading to singlet ($S=0$) and triplet ($S=1$) final spin states, can then be derived from the measurement according to the relations

$$\sigma_s \equiv \mathcal{K}\left[\left(\frac{3}{P_e}+1\right)(N^{\downarrow\Uparrow}+N^{\uparrow\Downarrow})-\left(\frac{3}{P_e}-1\right)(N^{\uparrow\Uparrow}+N^{\downarrow\Downarrow})\right], \tag{14}$$

$$\sigma_t \equiv \mathcal{K}\left[\left(\frac{1}{P_e}+1\right)(N^{\uparrow\Uparrow}+N^{\downarrow\Downarrow})-\left(\frac{1}{P_e}-1\right)(N^{\downarrow\Uparrow}+N^{\uparrow\Downarrow})\right]. \tag{15}$$

$\mathcal{K}$ is a normalization constant arising from the fact that the present $(e,2e)$ measurements are relative and not absolute.

D. Ionization from the oriented, excited states

For the ionization of excited states, where the target orientation is nonzero, the singlet and triplet ionization cross sections are dependent on the sign of the initial orbital orientation that changes with the reversal of the pump laser beam, i.e.,

$$\sigma_{s,\Uparrow(\Downarrow)} \equiv \mathcal{K}'\left[\left(\frac{3}{P_e}+1\right)N^{\downarrow\Uparrow(\uparrow\Downarrow)}-\left(\frac{3}{P_e}-1\right)N^{\uparrow\Uparrow(\downarrow\Downarrow)}\right], \tag{16}$$

$$\sigma_{t,\Uparrow(\Downarrow)} \equiv \mathcal{K}'\left[\left(\frac{1}{P_e}+1\right)N^{\uparrow\Uparrow(\Downarrow\downarrow)}-\left(\frac{1}{P_e}-1\right)N^{\downarrow\Uparrow(\uparrow\Downarrow)}\right]. \tag{17}$$

Here $\sigma_{s,\Uparrow(\Downarrow)}$ and $\sigma_{t,\Uparrow(\Downarrow)}$ stand respectively for the initial atomic-state resolved singlet and triplet cross sections for positive $\Uparrow$ $(m_F=+3, m_L=+1)$ and negative $\Downarrow$ $(m_F=-3, m_L=-1)$ target orientations. As noted above, for the reaction kinematics employed in the present measurements (Fig. 1), the ionization cross section from the state $m_L=0$ is zero.

It should be noted that the relationship between $\mathcal{K}$ and $\mathcal{K}'$ was determined experimentally in the present measurements as both the ground- and excited-state signals were collected simultaneously under identical experimental conditions. This was achieved by performing separate measurements, with the laser on and off respectively, to determine the excitation fraction according to the procedure described in a previous publication [5]. Thus the ground- and excited-state cross sections presented here for each of the three kinematical arrangements are determined within a single normalization factor. However, cross normalization of the experimental data between the three experiments has not been carried out. Thus a separate normalization factor relates the relative experimental to the theoretical cross sections in each of the three kinematical arrangements.

To relate the measured count rates with the tensorial parameters we have introduced above, we group them in the following way:

$$\sigma_{av} = \mathcal{K}'[N^{\uparrow\Uparrow}+N^{\uparrow\Downarrow}+N^{\downarrow\Uparrow}+N^{\downarrow\Downarrow}] = \mathcal{K}' N_\Sigma, \tag{18}$$

$$A_{orb} = \frac{1}{N_\Sigma}[N^{\uparrow\Uparrow}+N^{\downarrow\Uparrow}-N^{\uparrow\Downarrow}-N^{\downarrow\Downarrow}], \tag{19}$$

$$A_{mag} = \frac{1}{N_\Sigma P_e}[N^{\uparrow\Uparrow}+N^{\uparrow\Downarrow}-N^{\downarrow\Uparrow}-N^{\downarrow\Downarrow}], \tag{20}$$

$$A_{m,o} = \frac{1}{N_\Sigma P_e}[N^{\uparrow\Downarrow}+N^{\downarrow\Uparrow}-N^{\uparrow\Uparrow}-N^{\downarrow\Downarrow}]. \tag{21}$$

As shown below these quantities are independent and fully sufficient to characterize the ionization dynamics, for they are directly related to the tensorial parameters introduced above.

In terms of singlet and triplet cross sections the parameters (18)–(21) are readily re-expressed as

$$\sigma_{av}=[(3\sigma_{t,\Downarrow}+\sigma_{s,\Downarrow})+(3\sigma_{t,\Uparrow}+\sigma_{s,\Uparrow})]/4, \tag{22}$$

$$A_{orb}=[(3\sigma_{t,\Uparrow}+\sigma_{s,\Uparrow})-(3\sigma_{t,\Downarrow}+\sigma_{s,\Downarrow})]/(4\sigma_{av})$$

$$=\frac{(3\sigma_{t,\Uparrow}+\sigma_{s,\Uparrow})-(3\sigma_{t,\Downarrow}+\sigma_{s,\Downarrow})}{(3\sigma_{t,\Downarrow}+\sigma_{s,\Downarrow})+(3\sigma_{t,\Uparrow}+\sigma_{s,\Uparrow})}, \tag{23}$$

$$A_{mag}=[(\sigma_{s,\Downarrow}-\sigma_{t,\Downarrow})-(\sigma_{s,\Uparrow}-\sigma_{t,\Uparrow})]/(4\sigma_{av})$$

$$=\frac{(\sigma_{s,\Downarrow}-\sigma_{t,\Downarrow})-(\sigma_{s,\Uparrow}-\sigma_{t,\Uparrow})}{(3\sigma_{t,\Downarrow}+\sigma_{s,\Downarrow})+(3\sigma_{t,\Uparrow}+\sigma_{s,\Uparrow})}, \tag{24}$$

$$A_{m,o}=[(\sigma_{s,\Downarrow}-\sigma_{t,\Downarrow})+(\sigma_{s,\Uparrow}-\sigma_{t,\Uparrow})]/(4\sigma_{av})$$

$$=\frac{(\sigma_{s,\Downarrow}-\sigma_{t,\Downarrow})+(\sigma_{s,\Uparrow}-\sigma_{t,\Uparrow})}{(3\sigma_{t,\Downarrow}+\sigma_{s,\Downarrow})+(3\sigma_{t,\Uparrow}+\sigma_{s,\Uparrow})}. \tag{25}$$

Furthermore, one can write the singlet and the triplet cross sections in Eqs. (22)–(25) in terms of direct and exchange-scattering amplitudes and retrieve the formalism presented in Ref. [5].

For ionization of the isotropic $3s$ ground state ($J=1/2$), we have

$$\sigma_{av}^{S}=\mathcal{K}[N^{\uparrow\Uparrow}+N^{\uparrow\Downarrow}+N^{\downarrow\Uparrow}+N^{\downarrow\Downarrow}] \tag{26}$$

$$=(3\sigma_t+\sigma_s)/4, \tag{27}$$

$$A_{m,o}^{S}=\frac{\sigma_s-\sigma_t}{3\sigma_t+\sigma_s}. \tag{28}$$

Here σ_{av}^{S} and $A_{m,o}^{S}$ are the forms of σ_{av} and $A_{m,o}$ for the ionization of an isotropic state and A_{orb} and A_{mag} are zero in this case. Since we neglected spin-orbit interactions it is straightforward to deduce from Eq. (13) that only the tensorial parameters Λ_{00}^{00} and Λ_{00}^{11} are finite and are respectively proportional to the spin-averaged cross section (σ_{av}^{S}) and spin asymmetry ($A_{m,o}^{S}$) [for $J=1/2$ the expansion (13) contains four terms].

As mentioned above, for the present case of a polarized electron beam impinging onto a polarized target with $J=3/2$ the equation (13) consists of eight terms. However, due to the neglect of spin-orbit interactions only four terms are independent and are related to the quantities (22)–(25) as follows: $\sigma_{av}=\sqrt{2}\Lambda_{00}^{00}$, $A_{orb}=-\sqrt{5}/2\Lambda_{00}^{10}/\Lambda_{00}^{00}$, $A_{mag}=-\frac{1}{2}\Lambda_{00}^{01}/\Lambda_{00}^{00}$, and $A_{m,o}=\sqrt{5}/4\Lambda_{00}^{11}/\Lambda_{00}^{00}$. These relationships reveal that the four parameters (22)–(25) are independent and sufficient to fully characterize the ionization dynamics for the present arrangement. In addition, they possess well-defined transformation properties that are readily deduced from their rank: The parameter σ_{av} is a scalar that describes the ionization cross section averaged over the projections of the electrons' spins and the sense of orbital rotation and is independent of the helicity of the laser light. The quantity A_{orb}, defined for a beam of *unpolarized* electrons, is proportional to the spin-averaged *orbital dichroism*. It is a polar vector with respect to inversion of the laser's helicity but a scalar in the spin space of projectile electron, and results from the dependence of the ionization cross section on the *orientation* of the atomic target ensemble.

In contrast the tensorial parameter A_{mag}, hereafter referred to as the *magnetic dichroism*, changes sign when the polarization of the incoming electron beam is inverted but remains invariant under a change of the helicity of the photon [cf. Eq. (20)]. It describes a spin up-down asymmetry for a polarized beam of electrons from an *aligned* ensemble of target atoms. Its origin lies in the m_L dependence of the ionization cross section both in the singlet- and triplet-spin channels. If the individual singlet and triplet cross sections show no m_L dependence, i.e., if $\sigma_{s/t,\Uparrow}=\sigma_{s/t,\Downarrow}$, the magnetic dichroism vanishes, as can be directly deduced from Eq. (24). A similar effect appeared in the electron impact excitation process and the ionization of closed-shell systems by polarized electrons in presence of a spin-orbit interaction and was categorized as ''fine structure effect'' [21].

The fourth independent tensorial component $A_{m,o}$ is needed to fully characterize the present measurements. It is an exchange-induced antiparallel/parallel spin asymmetry and as such changes sign if the helicity of the photon is flipped or if the polarization of the incoming beam is inverted, as is clear from Eq. (21). In contrast to the spin asymmetry $A_{m,o}^{S}$ [cf. Eq. (28)], which results from the electron-impact ionization of spin-polarized electrons from spin-polarized targets with no orbital orientation [9], the parameter $A_{m,o}$ is influenced in a subtle way by the dependence of the singlet and the triplet cross sections on the orbital orientation of the initially polarized target.

This is reflected in a symmetry behavior of $A_{m,o}$ different from that of $A_{m,o}^{S}$. For example, for ionization from isotropic states in the doubly symmetric geometry (i.e., $\theta_a=\theta_b$ and $E_a=E_b$) the triplet ionization amplitude vanishes due to its odd symmetry behavior with respect to exchange of the two escaping electrons, and $A_{m,o}^{S}$ tends to unity [cf. Eq. (28)], as shown below [Fig. 5(b)]. This is because the experiment in the doubly symmetric configuration is invariant under a π rotation with respect to the incoming beam direction, but the triplet amplitude must change sign due to symmetry that imposes a node on the triplet scattering amplitude at this geometry.

In contrast, for oriented targets the triplet cross sections are generally finite in the case of doubly symmetric kinematics [6]. The origin of this effect is that the symmetry of space is broken by the presence of a defined direction in space (the target orientation induced by the circularly polarized laser beam). Therefore, the exchange of the two electrons does *not* correspond in this case to a symmetry operation under which our experiment is invariant (π rotation around the incoming beam axis.) Therefore $A_{m,o}$ does not need to tend to unity in the doubly symmetric kinematics. On the other hand, if the partial cross sections $\sigma_{t,\Uparrow/\Downarrow}$ vanish for the doubly symmetric

kinematics the experiment becomes invariant under a π rotation around the incoming beam leading to a vanishing triplet cross section and therefore $A_{m,o} \rightarrow 1$, as readily deduced from Eq. (25). Within the first Born approximation this is the case when the wave vector of the photon, the momentum transfer vector, and the vector momentum of the secondary electron are linearly dependent, i.e., are confined to the same plane. In the plane-wave impulse approximation (PWIA), i.e., when $\Psi_{\mathbf{k}_a \mathbf{k}_b}$ is modeled by two independent plane waves, the orbital dichroism vanishes identically, therefore the parameters A_{orb} and A_{mag} are identically zero and the asymmetry parameter $A_{m,o}$ reduces to the form (28) of $A^S_{m,o}$. This gives a hint of the high-energy behavior of the tensorial components (18)–(21) where the PWIA may be regarded as satisfactory.

IV. EXPERIMENTAL DATA AND COMPARISON WITH THEORY

The tensorial parameters given in Eq. (13) contain all the necessary information on the collision dynamics while the state multipoles describe the geometry of the excited state as prepared by the experiment. In principle, the dynamical tensorial parameters Λ^{ij}_{00} can be further expanded in terms of multipolar harmonics [20] that depend on the relevant vectors of the problem (the momentum vector direction of the electrons and the spin polarization vector of the incoming electron). This procedure is helpful for a general symmetry analysis but does not yield the actual values of the tensorial components that can be compared with experiments. For the evaluation of Λ^{ij}_{00} a dynamical model is needed to calculate the state-resolved singlet and triplet cross sections as is clear from Eqs. (22)–(25). In this work we utilize four standard calculational schemes: The PWIA and the first Born approximation (FBA) [3], the DWBA [13,3], and the DS3C [14]. All these approximations reduce the scattering from the Na atom to a three-body problem by considering only the active (valence) electron of the Na atom. The details of these models as applied to the present problem have been discussed in a previous work [5] and are not repeated here. As indicated by Eq. (9) the central quantity to be calculated is the transition matrix element $\mathcal{M}^J_M = \langle \chi_{SM_S} \Psi_{\mathbf{k}_a \mathbf{k}_b} | V | \varphi_{\mathbf{k}_0 m_s} \Phi_{JM} \rangle$. The initial state can be obtained from a pseudopotential approach [22,23] (as in the DS3C, the FBA, and the PWIA calculations) or from a standard Hartree-Fock method [24,25] (as employed by the DWBA method). A more serious problem is to find appropriate expression for the three-body final state $\langle \Psi_{\mathbf{k}_a \mathbf{k}_b} |$ (two continuum electrons in the field of Na^+). In the PWIA the interaction of these two electrons with the residual ion is neglected altogether as well as their mutual coupling, whereas within the FBA one accounts for the interaction of one of the electrons (the slow one) with Na^+ and neglects other final-state interactions. The DWBA approach accounts for the short- and long-range interactions of both of the electrons with the field of the ion [3,13]. The electron-electron interaction is, however, discarded from the treatment.

Finally, within the DS3C method the three-body system in the final state is considered as the sum of three decoupled two-body subsystems (the electron-electron, the electron-Na^+ and the electron-Na^+ two-body subsystems). The coupling of these three two-body subsystems is included in the theory via dynamical screening of the interaction strength of each of the three individual two-body subsystems [14]. From the nature of interactions included or omitted in each of these dynamical models one can deduce roughly the region where they are expected to perform reasonably well: The PWIA is a high-energy approximation for short-range potentials and as such is expected to perform well when the electron velocities are very large (compared to the typical velocity of the initially bound valence electron). The use of the FBA is sensible when one of the secondary electrons is very fast. The DWBA is justified when the electron-electron interaction is weak. This is the case when the relative velocities of the two final-state electrons are large and their absolute velocity values are not too small. Therefore the DWBA is not expected to describe as well the lower-energy results of those presented in this paper. The DS3C is designed to account explicitly for the electron-electron interaction in the presence of the residual ion. It does neglect, however, certain aspects of the three-body interactions that become more important at lower energies [19]. For isotropic targets the DS3C theory has been quite successful when compared to experiments [26]. It should be noted, however, that these arguments concerning the rough range of validity of the four dynamical models are based on the experience with isotropic targets. As shown here for scattering reactions involving polarized species the situation is more involved and arguments based only on the charge scattering dynamics (as dictated by the total electrostatic potential) may not be appropriate.

In Fig. 2 we compare the results of measurement with theory for the quantities (22)–(25) corresponding to ionization of the excited-state $3p$ electrons. Here the theoretical results have been averaged over the 6 eV experimental energy band as described in Sec. II. In Fig. 2(a) the averaged cross section data is presented. To facilitate comparison of theory with experiment, the experimental data have been normalized to the DS3C theory and the FBA and PWIA results scaled down by a factor of three. Obviously none of the theories describe accurately all the details of all of the parameters. It is particularly interesting to note that even under conditions where the FBA model could be expected to work reasonably well, namely, at a moderately high value of incident energy ($E_0 = 151$ eV) and in a kinematical regime encompassing the (classical) binary collision region, unsatisfactory agreement with experiment is observed. We remark that for isotropic targets and at such moderate energies the FBA, the DWBA, and the DS3C all give satisfactory results as compared to experiments [13,3,26] (see also Fig. 4).

The global trends in Fig. 2(a) can to some extent be understood by the following considerations. Analyzing the PWIA results we deduce that the main peaks in σ_{av} are due to a binary collision between the projectile electron and the valence $3p$ electron. The nodal structure of the initial-state P wave function at zero momentum results in a minimum in the cross section at the direction of momentum transfer at around 64°. The other three theories, in contrast, show only some small evidence for a minimum around this direction.

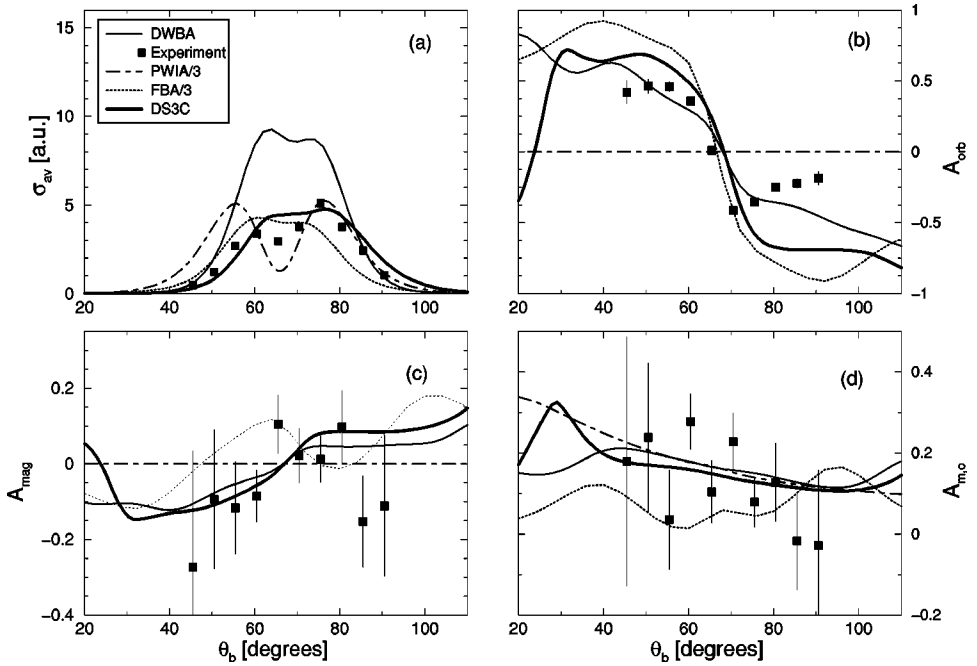

FIG. 2. Comparison of the measured and calculated cross section parameters σ_{av} (a), A_{orb} (b), A_{mag} (c), and $A_{m,o}$ (d) [see Eqs. (22)–(25)], for ionization from the oriented and excited $3p$ state of Na with polarized electrons. The incident beam energy $E_0=151$ eV and the mean energy of the detected fast scattered electrons $\overline{E_a}=127$ eV with corresponding scattering angle $\theta_a=20°$. The cross sections are plotted as a function of the slow electron scattering angle θ_b. The experimental average cross section [here seen in (a)] has been normalized to the DS3C theory. Solid and light lines are respectively the DS3C and DWBA calculations, and the short and long dashes are respectively the FBA ($\times 1/3$) and PWIA ($\times 1/3$) calculations.

This effect can be understood by considering the target-state resolved ionization cross sections (not shown) for which the orientation state of the target ensemble is resolved ($m_F=+3$ or $m_F=-3$), but for which the spin of the incident electrons is averaged. In the case of the PWIA, both target-state-resolved cross sections have exactly the same structure as that displayed in Fig. 2(a). This is because the orbital dichroism vanishes identically within the PWIA [cf. Fig. 2(b)]. For each of the other three theories, the target-state-resolved cross sections reveal a similar minimum to the PWIA. However, the minimum is shifted in angle due to the finite values of orbital dichroism present in each theory. When summing these cross sections over the target orientation state to obtain σ_{av}, the minimum is filled up, resulting in the angular behavior for σ_{av} seen in Fig. 2(a). Obviously, an accurate description of this effect of reduction in the depth of the cross section minimum due to angular shifts in the associated target-state-resolved cross sections depends upon a good description of orbital dichroism that is quantified in Fig. 2(b).

Figure 2(b) makes clear that a model that is capable of describing the charge-scattering dynamics may be completely inappropriate to simulate the orbital dependence of the scattering. In particular the PWIA model, while yielding some qualitative aspects of σ_{av} in Fig. 2(a), predicts identically vanishing orbital dichroism in a region where experiment indicates large finite values for this quantity.

The FBA results perform only marginally better than the PWIA in describing the shape of σ_{av}; however, this approximation does succeed in roughly predicting the shape of the experimentally derived orbital dichroism A_{orb} as seen in Fig. 2(b). Indeed, the FBA model predicts an exact reflection symmetry for the target-state-resolved cross sections about the direction of the momentum transfer $\vec{q}$ [7]. $\vec{q}$ occurs at $\theta_b\approx 64°$ in the present case, about which the experimental data is seen to show approximate reflection symmetry as θ_b is varied. This reflection symmetry about the momentum transfer direction is also apparent in the structure of A_{orb} as seen in Fig. 2(b), with a vanishing value occurring when θ_b coincides with this direction. Indeed the experimental values and all the results of the other theories indicate a vanishing value for A_{orb} around the direction of the momentum transfer, in accord with the FBA. In general, however, all theories fail to reproduce accurately the experimental findings over the full range of scattering angles θ_b over which measurement was performed. This is remarkable insofar as it is generally assumed that the kinematic range over which dynamical models are applicable can be judged from the magnitude of the momentum transfer and the kinetic energies of the particles involved.

In fact, this common wisdom is confirmed by the results for the averaged cross section parameter from isotropic targets (Fig. 4), but obviously ignores the importance of the orbital orientation effects that are quantified by A_{orb} [Fig. 2(b)].

The source of the deviation between the DS3C and the experiments for A_{orb} at larger ejection angles θ_b is most likely an oversimplified description of the Na atom that is based on the pseudopotential method [23]. The reason for

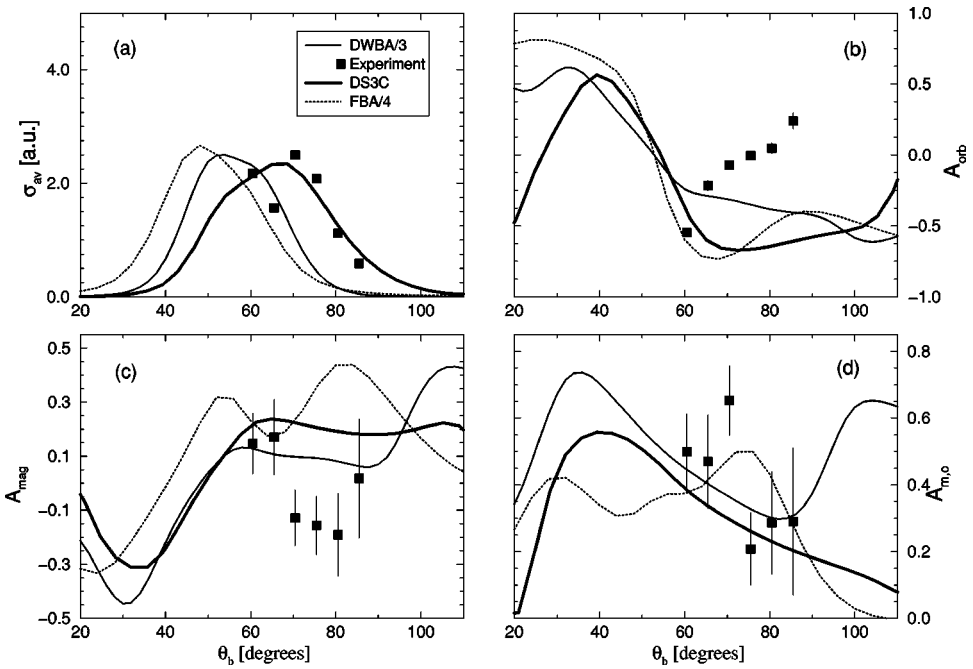

FIG. 3. Comparison of the measured and calculated cross section parameters σ_{av} (a), A_{orb} (b), A_{mag} (c), and $A_{m,o}$ (d) for $E_o=62$ eV, $\overline{E_a}=40.5$ eV and $\theta_a=20°$. Details as in Fig. 2 except that the PWIA results are now omitted and new multiplicative factors of 1/3 and 1/4 now apply to the DWBA and FBA theoretical cross sections, respectively.

this proposition is that the DS3C results for a hydrogenic target, with the same kinematics as in Fig. 2, deviate considerably from those for sodium. Of all the models presented, the DWBA provides the best description of the parameter A_{orb}, suggesting that final state electron-electron correlation may not play a significant role under these kinematics.

In Fig. 2(c) the parameter A_{mag} is shown. The experimental error bars are much larger in this figure [and in Fig. 2(d)], as both A_{mag} and $A_{m,o}$ are spin resolved quantities that can only be derived from the experimental counts after first extracting from the data contributions from the unpolarized fraction of the primary beam (76% for the experiments performed here). The employed extraction procedure significantly increases the statistical errors for low values of beam polarization. The physical origin of the structures revealed by A_{mag} are made clearer by expressing it in terms of the direct and exchange amplitudes

$$A_{mag}\propto\{\mathrm{Re}(f_{m_L=+1}g^*_{m_L=+1})-\mathrm{Re}(f_{m_L=-1}g^*_{m_L=-1})\}/\sigma_{av},$$

where f_{m_L} and g_{m_L} are the state-resolved direct and the exchange amplitudes. This relation makes clear that A_{mag} is in fact an exchange-induced quantity and it diminishes if an interference between g_{m_L} and f_{m_L} is unlikely, e.g., if $|g_{m_l}|/|f_{m_l}|\rightarrow 0$. When the direction of the ejected electron coincides with the direction of the momentum transfer (i.e., when $\theta_b\approx 64°$) the direct scattering amplitude $|f_{m_l}|$ predominates [27] and hence A_{mag} becomes small, and it increases for larger deviations from $\theta_b\approx 64°$ where exchange scattering can become significant. The four theories give significantly different dependences of A_{mag} on θ_b. The PWIA gives $A_{mag}=0$. The FBA gives fair agreement, considering the simplicity of the model, whilst the DWBA and DS3C perform only slightly better with similar behaviors over most of the angular range.

Figure 2(d) shows the results for the spin asymmetry $A_{m,o}$. This parameter can as well be written in terms of the direct and exchange amplitudes f_{m_L} and g_{m_L} as

$$A_{m,o}\propto\{\mathrm{Re}(f_{m_L=+1}g^*_{m_L=+1})+\mathrm{Re}(f_{m_L=-1}g^*_{m_L=-1})\}/\sigma_{av}$$

(note that in the present geometry the scattering from the state $m_L=0$ does not contribute). In the binary collision regime, which is of concern here, we can expect that in general $|f|$ will dominate (over $|g|$) so that $A_{m,o}$ is also generally small [27]. (With decreasing incident energies the contribution of the exchange scattering becomes more relevant [cf. Fig. 3(d)]. Within the error bars all theories perform satisfactorily. We recall here that this parameter reduces to the well-known spin-asymmetry $A^S_{m,o}$ when an isotropic target is employed. This illustrates again the importance of state-selective studies for the assessment of scattering theories with the PWIA performing reasonably for σ_{av} and $A_{m,o}$ but completely failing for the other two parameters.

In Fig. 3 the incident energy is lowered to 64 eV. Again the experimental average cross section data seen in Fig. 3(a) has been normalized to the DS3C theory, the FBA calculation divided by 4 and the DWBA calculation by 3 to facilitate comparison of theory and experiment. Due to the electron-electron interaction the binary peak is shifted from the direction of the momentum transfer vector (50°). The FBA and DWBA do not account for the electron-electron repulsion and consequently the shift of the binary peak is not accurately reproduced by those two models. The DS3C calculation, on the other hand, which does account for electron-electron interaction in the final state, provides a much better estimate of the shape of the averaged cross section. On the other hand, it is unable to predict the dip in this cross section around 65° as evident in the experimental data. It is noted that the DWBA overestimates the absolute value of the cross sections with respect to the DS3C. This behavior is in line

with the observation made for isotropic targets. However, as the present experimental cross sections are not determined on an absolute scale, the relative merits of the two theories cannot be assessed on the basis of their absolute values by comparison with experiment. The PWIA fails completely in this kinematical region and hence its results are not shown here. None of the theoretical models predict correctly the behavior of the orbital dichroism. In particular the DS3C theory, which provided a moderate description of the unpolarized cross section, is at complete variance with the experimental values. This demonstrates that further theoretical efforts, in particular towards improving the initial-state description, are needed. On the other hand, the present comparison endorses the importance of state-resolved ionization cross sections as an additional independent test for theories. The agreement between theory and experiment, as far as the magnitudes of the parameters A_{mag} and $A_{m,o}$ are concerned, can be considered as fair; however, the experimental error bars are large in these cases and future experimental advances are required to allow more precise conclusions in this regard. The results for $E_0=83$ eV and $\overline{E_a}=\overline{E_b}=40$ eV were presented previously [6] and will not be discussed here.

Figures 4(a)–4(c) show the singlet and triplet ionization cross section for the $3s$ ground state. The spin-averaged cross sections are shown in the insets, where both the DS3C and FBA results are shown. In case of Figs. 4(a), 4(b), and 4(c) the FBA results are scaled down respectively by the factors of 2, 3, and 4 to allow for shape comparison. As mentioned above, the absolute values of the cross sections for $3s$ and $3p$ ionization are not determined by measurement. However, both their relative values at the same kinematics, as well as the ratio of the singlet-to-triplet scattering cross sections are determined. In other words, whilst the values of the constants $\mathcal{K}'$ and $\mathcal{K}$ in Eqs. (18),(26) are not known, the ratio $R=\sigma_{av}^S/\sigma_{av}$ is determined by the experiments along with the absolute values of all the asymmetry parameters. To contrast theory with experiment it suffices to compare the value of R at one angular position. For the incident energy $E_0=151$ eV at $\theta_b=75.5°$ we obtain the experimental ratio $R=2.49\pm0.05$ whereas the DS3C theory gives a ratio of $R=0.96$. For $E_0=64$ eV at $\theta_b=60.5°$ the experiment yields $R=1.12\pm0.04$, compared with the DS3C value of $R=0.85$. Finally, for the incident energy $E_0=83$ eV at $\theta_b=50.5°$ we obtain the experimental ratio $R=1.81\pm0.09$. The theoretical DS3C value for R under this kinematics is not available. The values of this ratio for all other theories are readily obtained from the figures.

As expected from the repulsive nature of the electron-electron interaction (not included in the FBA) the binary peak position of the DS3C angular distributions is shifted towards larger angles as compared to the FBA results. This shift increases with decreasing incident energy since the strength of the electron-electron final-state interaction increases.

Generally, the agreement between the DS3C and FBA theories and experiment is quite good both with regard to the shape of the cross sections and to the relative magnitudes of the singlet verses triplet cross sections. At the lowest energy measured here ($E_0=64$ eV) the experiment shows a subsidiary structure around $\theta_s=75°$ that neither theory can describe.

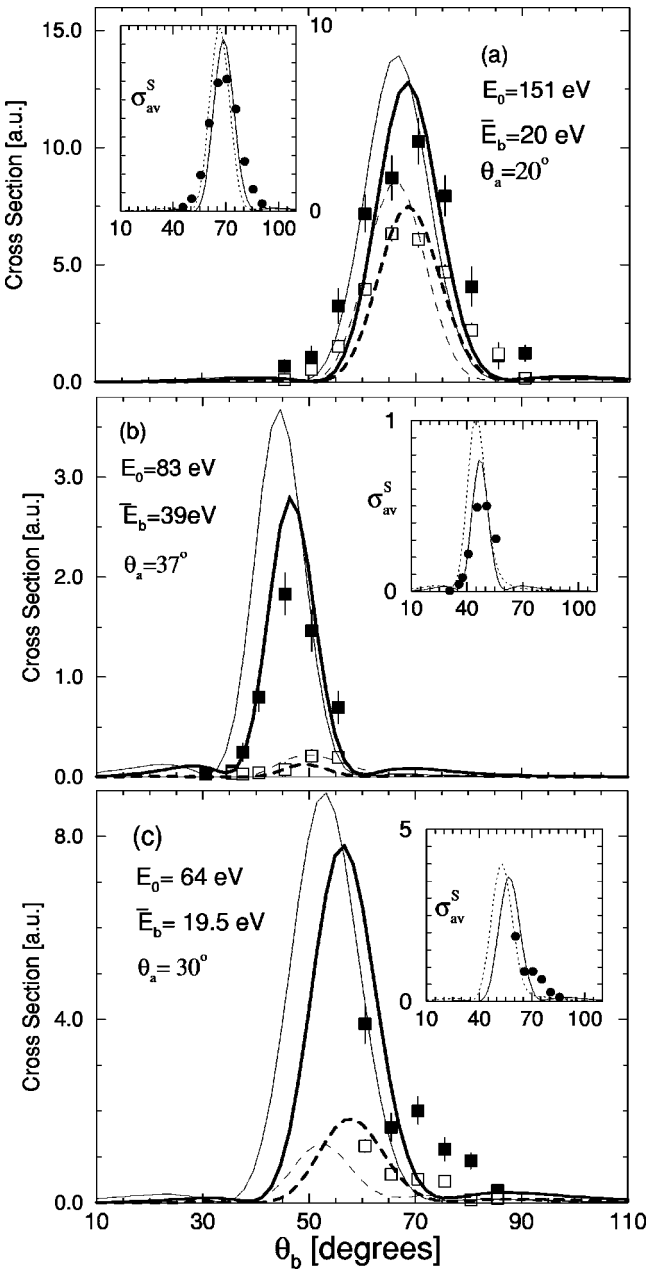

FIG. 4. Comparison of the measured and calculated DS3C singlet σ_s (solid squares and lines) and triplet σ_t (open squares and dashed lines) cross sections for the ionization of Na ground-state atoms at the indicated kinematics. The FBA calculations have been respectively scaled down by factors of 2, 3, and 4 in (a), (b), and (c) and their corresponding insets. The insets show the spin-averaged cross sections σ_{av}^S (DS3C solid and FBA dotted lines).

The FBA performs satisfactorily in shape for the spin-averaged cross sections (insets). This shows once again the importance of state-resolved measurements in revealing the details of the scattering dynamics.

Finally, in Fig. 5 we present the spin-asymmetry parameter $A_{m,o}{}^S$ for the ground state. The general structure and the

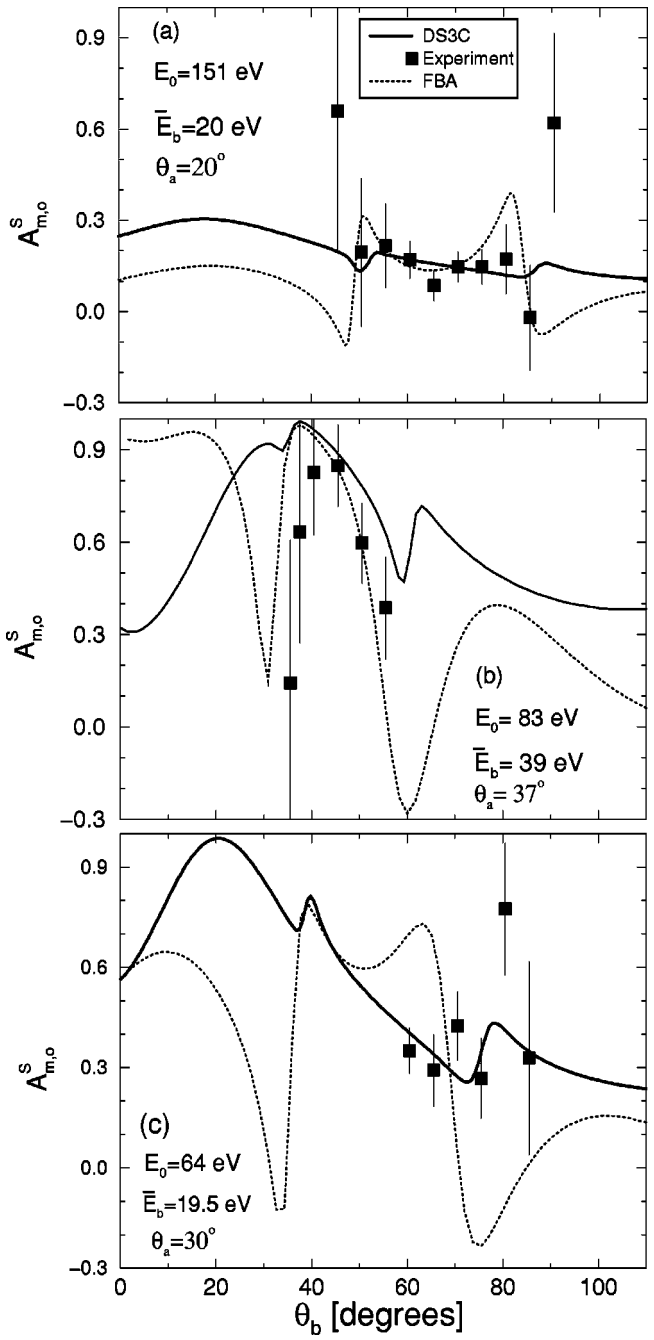

FIG. 5. Comparison of experimentally deduced and calculated spin asymmetries $A_{m,o}{}^{S}$ for the ionization of spin-polarized ground-state sodium atoms by spin-polarized electrons. Results for DS3C and FBA calculations are indicated respectively by solid and dotted curves.

absolute value of the spin asymmetry is reproduced by the theories. At $E_0=151$ eV a small spin asymmetry is expected, and this is confirmed by experiment. This is because exchange scattering in this binary collision region at high energies and under asymmetric energy-sharing conditions is expected to be small. Nevertheless, the spin asymmetry is clearly nonzero and reveals some sharp structures that can be associated with the behavior of the singlet and triplet cross sections at these angles. Clearly, more experimental data are needed in these regions to confirm the existence or nonexistence of these structures.

For the case $E_0=83$ eV, the triplet scattering vanishes at the angular position $\theta_b=37°$ for the doubly symmetric kinematic, as stated above. In this case the spin asymmetry tends to unity as confirmed both by theory and experimental data.

As expected the deviations between the FBA and the DS3C becomes more pronounced at lower energies. This is illustrated in Fig. 4(c) where the FBA fails badly to reproduce the absolute value of the spin asymmetry. Obviously, more experimental data are desirable to obtain a clear picture of the angular dependence of the spin asymmetry at this low energy.

V. CONCLUSION

We have carried out $(e,2e)$ cross sections measurements on sodium where the (spin and orbital) angular-momentum-projection state of the projectile and target are determined prior to the collision. The measurements involve the ionization of the

$$3s^1\ \ ^2S_{1/2}(F=2,m_F=+2\ \text{ or }\ m_F=-2)$$

and the

$$3p^1\ \ ^2P_{3/2}(F=3,m_F=+3\ \text{ or }\ m_F=-3)$$

hyperfine states by spin-polarized electrons at medium-impact energies.

To provide a general description we have developed a tensorial recoupling scheme that factorizes the cross sections into components characterized by their spherical transformation properties. In addition it allows decoupling of the preparation process of the laser-pumped target from the ionization dynamics.

For a comparison with the experimental results we performed calculations within the DWBA and the DS3C model (as well as the first Born approximation and the PWIA).

The results show that the initial-state resolved ionization cross section depends both on the relative spin projections of the incident and bound-state electrons and on the orientation of the initial atomic state. While the overall dependence of the experimental cross sections are reproduced by the two theoretical models, the lack of a detailed agreement demonstrates that state specific measurements provide a novel way to test the electron-electron scattering dynamics and the proposed theories for its description.

The theories can be improved by using improved descriptions of the initial state. Improvement in the experimental apparatus are underway by introducing new-generation electron analyzers, capable of measuring data simultaneously over a wide range of angles and energies for the final-state electron pair and by employing a polarized electron source of much improved degree of polarization P_e.

[1] P. Fulde, *Electron Correlations in Molecules and Solids* (Springer Verlag, Berlin, 1991).
[2] C. J. Joachain, *Quantum Collision Theory* (North-Holland Publishing Company, Amsterdam, 1975)
[3] I. E. McCarthy and E. Weigold, *Electron-Atom Collisions* (Cambridge University Press, Cambridge, 1995).
[4] A. Dorn, A. Elliot, J. Lower, E. Weigold, J. Berakdar, A. Engelns, and H. Klar, Phys. Rev. Lett. **80**, 257 (1998).
[5] J. Lower, A. Elliott, E. Weigold, S. Mazevet, and J. Berakdar, Phys. Rev. A **62**, 012706 (2000).
[6] J. Lower, E. Weigold, J. Berakdar, and S. Mazevet, Phys. Rev. Lett. **86**, 624 (2001).
[7] J. Berakdar and H. Klar, Phys. Rep. **340**, 473 (2001).
[8] J. Berakdar, Phys. Rev. Lett. **83**, 5150 (1999); S. N. Samarin *et al.*, *ibid.* **85**, 1746 (2000).
[9] G. Baum, W. Blask, P. Freienstein, L. Frost, S. Hesse, W. Raith, P. Rappolt, and M. Streun, Phys. Rev. Lett. **69**, 3037 (1992).
[10] M. Streun, G. Baum, W. Blask, J. Rasch, I. Bray, D. V. Fursa, S. Jones, D. H. Madison, H. R. J. Walters, and C. T. Whelan, J. Phys. B **31**, 4401 (1998); M. Streun, G. Baum, W. Blask, and J. Berakdar, Phys. Rev. A **59**, 4109 (1999).
[11] M. Streun, G. Baum, W. Blask, and J. Berakdar, Phys. Rev. A **59**, R4109 (1999).
[12] The terms orientation and alignment as used in this work are different from the conventions used by U. Fano and J. H. Macek, Rev. Mod. Phys. **45**, 553 (1973) for the polarization analysis of dipole radiation emitted from oriented and aligned targets. In the work by Fano and Macek the wave functions used to evaluate the tensorial components are eigenfunctions of angular momentum so that the Winger-Eckert theorem applies. This is not the case here, for this reason we simply refer to the rank of the respective tensor to identify orientational (rank is odd) are alignment (rank is even) parameters.
[13] I. E. McCarthy, Aust. J. Phys. **48**, 1 (1995).
[14] J. Berakdar, Phys. Rev. A **53**, 2314 (1996).
[15] A. Dorn, A. Elliott, J. Lower, S. F. Mazevet, R. P. McEachran, I. E. McCarthy, and E. Weigold, J. Phys. B **31**, 547 (1998).
[16] E. E. Campbell, H. Hülser, R. Witte, and I. V. Hertel, J. Phys. B **16**, 21 (1990).
[17] J. Lower and E. Weigold, J. Phys. E **22**, 421 (1989).
[18] K. Blum, *Density Matrix Theory and Applications* (Plenum, New York, 1981).
[19] J. Berakdar, A. Engelns, and H. Klar, J. Phys. B **29**, 1109 (1996).
[20] N. L. Manakov, A. V. Meremianin, and A. F. Starace, Phys. Rev. A **57**, 3233 (1998).
[21] S. Jones, D. H. Madison, and G. F. Hanne, Phys. Rev. Lett. **72**, 2554 (1994).
[22] M. Klapisch, Ph.D. thesis, University of Paris-sud, Orsay, 1969.
[23] M. Klapisch, M. Machholm, and E. Lawartowski, Z. Phys. D: At., Mol. Clusters **30**, 205 (1994).
[24] C. F. Fischer, Comput. Phys. Commun. **43**, 355 (1987).
[25] E. Clementi and C. Roetti, At. Data Nucl. Data Tables **14**, 177 (1974).
[26] J. Berakdar, Phys. Rev. A **56**, 370 (1997).
[27] C. J. Joachain, Comments At. Mol. Phys. **17**, 261 (1986).